

SLIM: An Improved Generalized Born Implicit Membrane Model

Julia Setzler,^[a] Carolin Seith,^[a] Martin Brieg,^[b] and Wolfgang Wenzel^{1*^[a]}

In most implicit continuum models, membranes are represented as heterogeneous dielectric environments, but their treatment within computationally efficient generalized Born (GB) models is challenging. Despite several previous attempts, an adequate description of multiple dielectric regions in implicit GB-based membrane models that reproduce the qualitative and quantitative features of Poisson–Boltzmann (PB) electrostatics remains an unmet prerequisite of qualitatively correct implicit membrane models. A novel scheme (SLIM) to decompose one environment consisting of multiple dielectric regions into a sum of multiple environments consisting only

of two dielectric regions each is proposed to solve this issue. These simpler environments can be treated with established GB methods. This approach captures qualitative features of PB electrostatic that are not present in previous models. Simulations of three membrane proteins demonstrate that this model correctly reproduces known properties of these proteins in agreement with experimental or other computational studies.

Introduction

Membrane proteins are essential to many biological activities. They catalyze the specific transport of metabolites and ions across the membrane, act as signal receptors and are involved in biological energy conversion.^[1] These functions are determined by the protein's structure, its dynamics, and interactions. Their understanding is crucial for drug design and treatment of diseases such as cancer, diabetes, or heart disease, which can be caused by malfunction of membrane proteins.^[2] While it is estimated that 20% to 30% of all genes encode membrane proteins,^[3] our knowledge about them is rather limited in comparison to proteins acting in aqueous solution, because the hydrophobic environment of membrane proteins poses a great challenge for experimental techniques such as X-ray crystallography^[1,4,5] and nuclear magnetic resonance spectroscopy.^[6]

Computer simulations can in principle help to understand the atomic mechanisms essential for these functions. Unfortunately, the high cost of an all-atom explicit membrane representation limits the timescales accessible by typical molecular dynamics simulations to the nanosecond range. Thus, many biological questions were out of reach for these simulations,^[7] because the underlying processes take place on the microsecond up to the second timescale.^[8] Despite recent progress in hard- and software, accessible timescales are still in the low microsecond range.^[9–13]

Approximate membrane models have been proposed to reduce the computational cost, wherefore they can provide either enhanced or more cost efficient sampling of biological processes.^[7,14] These models can be roughly grouped into two categories, either focusing on coarse-graining^[15–20] (for a recent review, see also Saunders et al.^[21]) or on implicit modeling of the membrane.^[22–33] For the latter category, there is a wide variety of models, ranging from strictly empirical ones,^[22] to

models based solely on the solvent accessible surface area (SASA),^[23,24] and those exploiting the separation of the solvation free energy into electrostatic and nonpolar contributions.

The electrostatic contribution can be approximated by Poisson–Boltzmann (PB) theory, where the membrane is modeled by different dielectric regions. Partial atomic charges induce polarization charges at the interfaces of these regions, which in turn interact with the partial atomic charges and so forth. While several PB methods have been implemented to treat the electrostatics of membranes,^[25,30–32] these models are computationally too expensive for the investigation of long timescales or extensive conformational samples. A large number of generalized Born (GB) models offer an approximation that is computationally less demanding.^[26,28,29,33–46] The interactions of partial atomic charges with the induced polarization charges are approximated by conformation dependent Born radii and a pairwise analytic formula.^[46] Unfortunately, GB models are limited to two dielectric regions by construction, which are typically chosen as the solvent and the solute. A membrane region with different dielectric properties can, therefore, not be incorporated into standard GB models.

[a] J. Setzler, C. Seith, W. Wenzel
Institute of Nanotechnology (INT), Karlsruhe Institute of Technology (KIT),
P.O. Box 3640, 76021 Karlsruhe, Germany
E mail: wolfgang.wenzel@kit.edu

[b] M. Brieg
Steinbuch Centre for Computing (SCC), Karlsruhe Institute of Technology
(KIT), P.O. Box 3640, 76021 Karlsruhe, Germany
Contract grant sponsor: DFG (to W.W.); Contract grant sponsor:
Landesgraduiertenfoerderung Baden Wuerttemberg and the HPC 5 project
of the Baden Wuerttemberg Stiftung (to M.B.); Contract grant sponsor:
Ministry of Science, Research and Arts and the Universities of the State
of Baden Wuerttemberg, Germany (for computational resources)

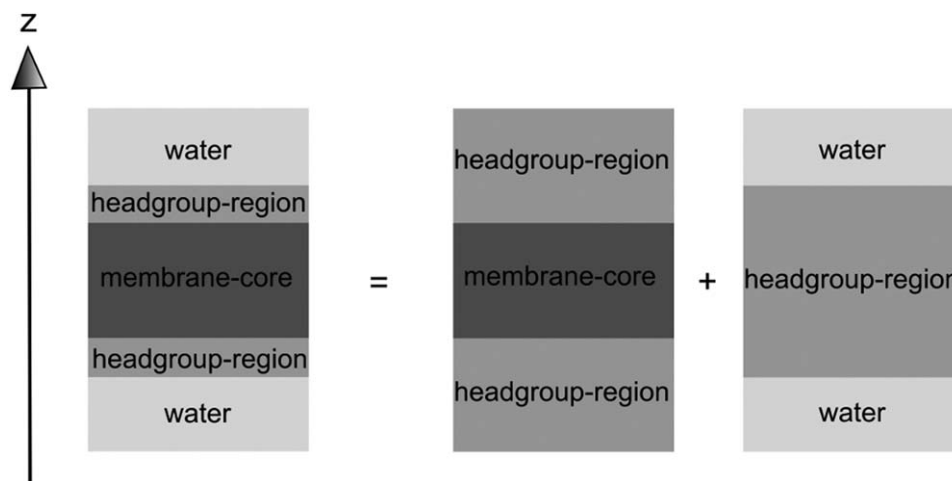


Figure 1. Sketch of decomposing a biological membrane model consisting of three different dielectric regions into a sum of two models with only two different dielectric regions each. For the latter two, the interactions between partial atomic charges and induced polarization charges at the dielectric interfaces can be approximated with already established GB implicit membrane models for two dielectric regions.

Spassov et al.^[26] investigated a model in which protein and membrane region are treated as a single region with the same dielectric constant. The influence of the membrane on electrostatic interactions is, thus, accounted for in the Born radii, which describe the overall conformation of the solute and its position relative to the membrane. Other models based on this work were published by Im et al.^[28] and Ulmschneider et al.^[33] A subsequent study with an explicit membrane representation demonstrated that this approximation is insufficient and that membranes should at least be modeled by one low dielectric slab flanked by an additional slab of intermediate dielectric constant. Otherwise transfer free energy errors of up to 14 kcal/mol per unit charge are introduced in the transition region between water and the membrane core.^[47] Therefore, new approaches to include multiple dielectric regions into the GB model are required.

An alternative approach by Tanizaki and Feig^[29] proposed that each atom is subject to a position dependent dielectric constant $\epsilon(\mathbf{r})$ that varies smoothly between the dielectric constant of the solvent ϵ_w and that of the membrane core region ϵ_c . While this method allows inclusion of any number of different dielectric regions to model biological membranes, it has some important artifacts: For example, the interaction of ions or charged protein regions on opposite sides of the membrane is not altered by its presence, which severely distorts the electrostatic interactions. Another example where such a model fails to predict energetically favored orientations of a simple transmembrane helix model is given in the PB comparison in the results section. An adequate description of multiple dielectric regions in the context of an implicit GB-based membrane model that reproduces the qualitative and quantitative features of PB electrostatics, thus, remains an unmet prerequisite of qualitatively correct implicit membrane models.

In this work, we present a novel scheme to decompose one environment consisting of multiple dielectric regions into multiple environments consisting of only two dielectric regions.

An example for this decomposition is depicted in Figure 1. Subsequently, these simpler dielectric environments can be treated with established GB implicit membrane methods for only two dielectric regions. We demonstrate that this approach captures all the qualitative features of PB electrostatics with good quantitative agreement. Thus, our approach provides an important prerequisite for correctly incorporating biological membranes in implicit solvent models.

The remainder of this article is structured as follows. The decomposition of the environment and the subsequent modeling of these simpler environments by GB terms are explained in detail in the chapter “SIMONA Layered Implicit Membrane Model”. The methods section describes the implementation of this approach into a forthcoming release of the SIMONA Monte Carlo simulation packages,^[48] as well as details of the Monte Carlo simulations performed in this work. The results and discussion section starts with a presentation of several PB test cases to demonstrate the good qualitative and quantitative agreement with our model, which cannot be achieved using other implicit membrane models. Further validation of our model to experimental data and simulation results by others is done by comparing Monte Carlo simulation results of three well-studied membrane proteins, Melittin, the transmembrane domain of the M2 protein and Glycophorin A.

SIMONA Layered Implicit Membrane Model

Our proposed implicit membrane model SLIM follows the usual separation of the solvation free energy into a polar part describing electrostatic effects and a nonpolar part^[49]

$$\Delta G = \Delta G_{\text{elec}} + \Delta G_{\text{NP}} \quad (1)$$

We model the electrostatic contribution to the solvation free energy of an interface between two dielectric regions using a GB model based on Still’s formula^[46]

$$\Delta G_{\text{GB}}(\varepsilon_d, V_d; \varepsilon_e, V_e; \{R\}_i) \approx \frac{\alpha}{2} \left(\frac{1}{\varepsilon_d} - \frac{1}{\varepsilon_e} \right) \sum_{\text{atoms } m, n} \frac{q_m q_n}{\sqrt{r_{mn}^2 + R_m R_n} \exp\left(\frac{r_{mn}^2}{4R_m R_n}\right)} \quad (2)$$

where $\{R\}_i$ is a set of atomic Born radii for the transition between the regions V_d and V_e with dielectric constants ε_d and ε_e , for example, the solute and solvent region. The distance between two atoms m and n is denoted by r_{mn} , the partial charge of an atom by q , and $\alpha = 331.84$ (Å kcal)/mol is a constant.

Unfortunately Still's original GB model and the extension of Spassov et al. can only model a system with exactly two different dielectric constants. The reason is that these models require the computation of Born radii for each atom, which describe the amount of polarization charge induced at one dielectric interface. To zeroth order, these Born radii can be computed using the Coulomb field approximation.^[39,50] As the induced surface charges on one interface do not only interact with the solute charges but also with themselves, higher order corrections and other methods have been developed to account for this effect.^[40,51] If the system contains more than one dielectric interface, there will be induced surface charges on all of these interfaces. Subsequently, the surface charges on one interface will also interact with those at another interface. While PB methods are able to account for this effect, it is not clear how to incorporate this effect into GB models.

To enable GB computations for multiple dielectric interfaces, we propose to decompose the electrostatic contribution of the solvation free energy for an environment consisting of N regions V_N with different dielectric constants ε_N into the sum of $N - 1$ GB terms

$$\Delta G_{\text{elec}}(\varepsilon_1, V_1; \varepsilon_2, V_2; \dots; \varepsilon_N, V_N) \approx \sum_{i=1}^{N-1} \Delta G_{\text{GB}}\left(\varepsilon_i, \bigcup_{f=0}^{f \leq i} V_f; \varepsilon_{i+1}, \bigcup_{g=i}^{g \leq N} V_g; \{R\}_i\right) \quad (3)$$

Thus, the electrostatic contribution to the solvation free energy of a dielectric interface between ε_i and ε_{i+1} is modeled by a GB term where all regions V_f with $f \leq i$ are assigned the dielectric constant ε_i and all regions V_g with $g > i$ are assigned dielectric constant ε_{i+1} .

By decomposing the complete system into several systems with only one dielectric interface, we neglect the problematic interaction of induced surface charges on different interfaces within GB models. This approximation requires that the induced surface charge distribution on one interface only has a small influence on the surface charge distribution on another interface. In general, this approximation may not hold. However, as we will show later, for a fixed geometry as used in implicit membrane models, it will be possible to alter each GB term on the right hand side of eq. (3), so that their sum still shows reasonable agreement with PB results obtained for the complete system.

To model a biological membrane in SLIM, we use the geometry proposed by Tanizaki and Feig.^[29] They represent the membrane's core region by a flat, infinite dielectric slab of thickness h_c and dielectric constant ε_c , surrounded on both

sides by a headgroup region with thickness h_h and dielectric constant ε_h . The latter is surrounded by infinite implicit water with a dielectric constant ε_w . Without loss of generality, we always assume the slabs perpendicular to the z-axis.

Following Spassov et al., we also assume the same dielectric constant for the protein as in the membrane core region,^[26] thus, the region V_c includes the membrane core as well as the protein interior. Using our proposed approximation on this environment, the electrostatic part of the solvation free energy decomposes into

$$\Delta G_{\text{elec}}(\varepsilon_c, V_c; \varepsilon_h, V_h; \varepsilon_w, V_w) \approx \Delta G_{\text{GB}}(\varepsilon_c, V_c; \varepsilon_h, V_h \cup V_w; \{R\}_1) + \Delta G_{\text{GB}}(\varepsilon_h, V_c \cup V_h; \varepsilon_w, V_w; \{R\}_2) \quad (4)$$

as depicted in Figure 1. So for the first GB term, we assign ε_c to the region V_c (the protein and membrane core regions), and ε_h to the headgroup region V_h and water region V_w . In the second term, ε_h is assigned to the protein and the membrane core V_c , as well as the headgroup region V_h , while the water region V_w has dielectric constant ε_w . While it is possible to use a different dielectric constant for the protein by adding another term to eq. (4), we have not investigated this possibility further in the work presented here.

Besides the electrostatic contribution, the nonpolar part of the solvation free energy in eq. (1) has to be also modeled. This is usually done by a SASA term that penalizes cavity formation in water depending on the number of water molecules in the first solvation shell, which is assumed to be proportional via the factor γ to the surface area of the cavity.^[52] To include the membrane into the nonpolar contribution of the solvation free energy, we follow the approach of Tanizaki and Feig^[29] and use a position dependent scaling function $S(z_m)$ that decreases the penalty of forming hydrophobic cavities for atoms located inside the membrane at position z_m and with SASA A_m .

$$\Delta G_{\text{NP}} = \gamma \sum_{\text{atoms } m} S(z_m) A_m \quad (5)$$

Methods

Implementation

To compute the Born radii in the presence of one low dielectric slab, as required by our SLIM model, we use the PowerBorn method due to its good accuracy and high performance.^[53] The Born radius R_m of an atom m at position \mathbf{r}_m is given by the R6 integral expression proposed by Grycuk^[51]

$$\frac{1}{R_m^3} = \frac{3}{4\pi} \int_{\text{water}} \frac{dV}{|\mathbf{r}_m - \mathbf{r}|^6} \quad (6)$$

where the integration region is the volume covered by water around the solute. PowerBorn's integration method consists of two steps. The water volume outside a bounding box around

the molecule is integrated using analytical formulas, while a numerical integration scheme is used for the water region inside the bounding box due to the complex solvent excluded surface. To exclude integration from the region of a low dielectric slab, we have slightly modified this scheme.

We achieve this by differentiating three cases. In the first case, the bounding box lies completely outside the slab. Therefore, we perform the usual Born radii integration of the PowerBorn method. Before converting the integrals via eq. (6) to the Born radii, we have to subtract the contributions $I_{\text{slab}}^{\text{outside}}$ of the low dielectric slab from the computed integrals. The R6 Integral over the infinite planar slab can easily be solved by converting the volume integral to surface integrals over the slab surfaces. Using cylindrical coordinates to solve the integral we arrive at

$$I_{\text{slab}}^{\text{outside}}(z_m, z_l, z_u) = \frac{\pi}{6} \frac{(z_m - z_u)}{(z_m - z_u)^4} \frac{(z_m - z_l)}{(z_m - z_l)^4} \quad (7)$$

where z_m is the z-coordinate of the atom in question, and z_l and z_u are the lower and upper z-positions of the slab boundaries.

In the second case, the bounding box is completely buried inside the slab. Hence, no numerical integration inside the bounding box is required. The only contribution $I_{\text{slab}}^{\text{inside}}$ to the Born radius integral then comes from the region outside the slab. Integration is done in analogy to the first case by converting the volume integral of eq. (6) to surface integrals,

$$I_{\text{slab}}^{\text{inside}}(z_m, z_l, z_u) = I_{\text{slab}}^{\text{outside}}(z_m, z_l, z_u) \quad (8)$$

In the last case, the bounding box intersects one or both surfaces of the slab. To exclude numerical integration inside the bounding box from regions that are also inside the slab, we construct a shifted bounding box outside the slab, so that its top or bottom side is aligned with the lower or upper surface of the slab respectively. If the bounding box touches both slab boundaries, we construct an aligned bounding box on each side of the slab. Afterwards, the usual numerical PowerBorn integration can be performed inside the bounding boxes. The region outside the bounding box is again treated analytically via surface integration. The surfaces are the five sides of the bounding box not aligned with the slab surface, and the slab surface excluding the square of the bounding box that lies within the slab surface. The integral I_{square} over one face of the bounding box is described by Brieg and Wenzel^[53] and the integral over the slab excluding the square is given by

$$I_{\text{slab}}^{\text{square}} = I_{\text{slab}}^{\text{inside}} - I_{\text{square}} \quad (9)$$

However, implementation of this contribution is not straightforward, since both terms on the right hand side of eq. (9) are divergent if an atom moves toward the slab surface and only their difference is finite. In that case, one can use a Taylor expansion of both terms whenever an atom at z_m is close to the slab surfaces at z_l or z_u . The divergent terms cancel out and only finite terms of the Taylor expansion remain.

To further improve agreement with PB calculations, PowerBorn radii are rescaled according to Brieg and Wenzel^[53]

$$\frac{1}{\tilde{R}} = \frac{a}{R} + b \quad (10)$$

with fit parameters a and b . Due to the presence of the low dielectric slab, very large Born radii above 20 Å are common in our SLIM model. To avoid saturation of the Born radii due to the nonvanishing parameter b , that would lead to an over-estimation of charged group interactions inside the slab, we repeated the fit procedure described by Brieg and Wenzel^[53] with fixed $b = 0$, $\epsilon_c = \epsilon_p = 2$, $\epsilon_w = 80$ and obtained $a = 1.130153$.

The Born radii computation and the evaluation of eq. (2) have to be done for every term on the right hand side of eq. (3). While this poses an extra cost to our model, efficient methods for Born radii evaluation and code parallelization can make up for this. The resulting implicit membrane model was added to the SIMONA^[48] Monte Carlo simulation package, thus, enabling simulations of membrane proteins.

We like to point out, that in the case of modeling the membrane with only one dielectric slab, our scheme resembles that of Spassov et al.,^[26] but uses a different underlying method to compute the Born radii. We also note that in the case where the membrane is far away from the protein, the slab contributions to the Born radii will be negligible, and therefore, all terms on the right hand side of eq. (3) or (4) will have the same set of Born radii. Since Still's formula in eq. (2) is additive if the same set of Born radii $\{R\}$ is used

$$\Delta G_{\text{GB}}(\epsilon_c, V_c; \epsilon_w, V_w; \{R\}) = \Delta G_{\text{GB}}(\epsilon_c, V_c; \epsilon_h, V_h; \{R\}) + \Delta G_{\text{GB}}(\epsilon_h, V_h; \epsilon_w, V_w; \{R\}) \quad (11)$$

SLIM converges to an implicit GB water model with dielectric constants ϵ_c for the protein and ϵ_w for water as the distance to the membrane tends to infinity.

Computation of the SASA A_m for the nonpolar contribution in eq. (5) to the solvation free energy is performed using the PowerSASA method.^[54] We use the nonpolar profile function $S(|z_m|)$ of Tanizaki and Feig without the oxygen correction,^[29] which was fitted to the free energy profile of pulling a completely neutral O_2 molecule through an explicit membrane.^[55] Therefore, this profile is independent of the model used for the electrostatic contribution to the solvation free energy. For membranes with thicknesses $h_m \neq 30.0$ Å, the original profile function is stretched or compressed, resulting in a new profile

$$\tilde{S}(|z_m|) = S\left(\frac{30.0}{h_m}|z_m|\right) \quad (12)$$

Although new profiles from explicit membrane calculations with varying thickness would be more accurate, this stretched profile should provide a reasonable estimate of the nonpolar contribution, which can be further improved if deemed necessary.

Monte Carlo simulations

PDB files were read in and processed by pdb2gmx from the Gromacs package,^[56] using the Amber99SB*-ILDN^[57-59] force

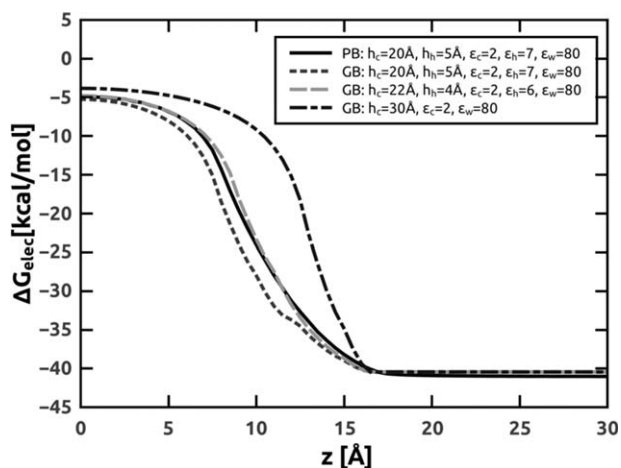


Figure 2. Comparison of the electrostatic solvation free energy profile from PB calculations (solid line) to our proposed GB based SLIM model with the same membrane parameters as in PB (dotted line), with modified membrane parameters (dashed line), and with only one low dielectric slab resembling the model of Spassov et al.^[26] (dot-dashed line) for pulling a single ion through a membrane.

field. The structures were energetically minimized using Gromacs. Resulting structures were used as input structures for SIMONA Monte Carlo simulations. No force field cutoffs were used during the simulations.

For every system and parameter set, 20 independent SIMONA simulations were performed at 300 K. Simulations were run for 20 million Monte Carlo steps except Glycophorin A, where 10 million steps were used. Monte Carlo moves included random rigid body rotations and translations as well as all backbone and side chain dihedral rotations. All dihedral moves used Gaussian distributions to determine the size of the move. The width of the Gaussian was 20°. Rigid body rotations were achieved by rotating the molecule around a random axis through its geometric center with a uniformly distributed rotation angle of up to 5°. Translations were generated by moving the rigid molecule along a random axis. The distance was distributed so that each translation inside a sphere of radius 1.4 Å was equally likely.

Results and Discussion

PB comparison

In the following, we report a set of increasingly complex validation simulations for the SLIM model. In one of the most straightforward tests, we compare results of the new model with PB calculations using the PBEQ solver.^[32,60] This allows us to examine how far the approximation in eq. (3) or (4) is justified and whether the decomposed terms need to be modified to achieve good agreement between our GB-based membrane model and PB results.

The self-energy, defined by the terms of eq. (2) with $m = n$, is tested by comparing the electrostatic solvation free energy profile of a single ion that is pulled through the membrane with respect to PB computations. We use the membrane geometry proposed by Tanizaki and Feig,^[29] with a core region

thickness of $h_c = 20.0$ Å and dielectric constant of $\epsilon_c = 2.0$. On either side is a $h_h = 5.0$ Å wide headgroup region with a dielectric constant of $\epsilon_h = 7.0$. The membrane is embedded in implicit solvent with a dielectric constant of $\epsilon_w = 80.0$. Figure 2 shows the results of this test for PB reference computations (solid line), our proposed membrane model using the same parameters as the PB model (dotted line), our GB-based SLIM model with modified membrane parameters $h_c = 22.0$ Å, $\epsilon_c = 2.0$, $h_h = 4.0$ Å, and $\epsilon_h = 6.0$ (dashed line), and a model analogous to Spassov et al.^[26] with only one membrane slab $h_c = 30.0$ Å, $\epsilon_c = 2.0$ (dot-dashed line).

For the latter, we observe a very steep transition into the membrane in agreement with the findings of Tanizaki and Feig.^[29] However, this steep transition due to the single slab does not agree with results computed using an explicit membrane representation.^[47] Our membrane model using the same membrane parameters as the PB calculations has a much smoother transition, but still shows some deviations to PB results in the core-headgroup transition region. However, this discrepancy may be eliminated by using our proposed GB method with modified thicknesses and dielectric constants. The modified parameters for the SLIM model are able to account for the neglected interaction of the induced surface charges at the different dielectric interfaces, as explained in the section “SIMONA Layered Implicit Membrane Model.”

As a single ion possesses a very simple geometry, this test is not very challenging. One can increase its difficulty by using a more complex molecular geometry. We have chosen the structure of Magainin (PDB code: 2MAG)^[61] and removed all except a single charge located at the C_α atom of Asn₂₂, which we set to the charge of a proton, to further test the self-energy term. The structure is again pulled through the membrane, but this time in three different orientations of the same conformation, and the charged atom of all three orientations is always kept at the same position, as shown in Figure 3a. The PB and GB self-energy profiles as function of the z -position of the charged atom in Figure 3b consistently show an energetic preference for conformations where the uncharged part of the structure is buried inside the membrane, if the charge is in or near the headgroup region. This preference vanishes as the charge is moved deeper into or further away from the membrane. The quantitative agreement between our proposed GB membrane model and PB results is also very good. The maximum deviation is 1.69 kcal/mol when using the modified thicknesses and dielectric constants.

We stress that models using a z -dependent Born radius scaling or a dielectric profile to incorporate the membrane, such as that proposed by Tanizaki and Feig,^[29] are by construction unable to reproduce these energetic preferences, because the z -position of the charged atom is the same for all three orientations. Therefore, models of such type would fail this test.

We also investigated the interaction terms of eqs. (2) and (4) by studying the electrostatic solvation free energies of two ions and subtracting the self-energy contributions. One ion was placed in the center of the core region while the other was placed 4 Å away in a direction parallel to the membrane plane. The profiles in Figure 4 were generated by moving the

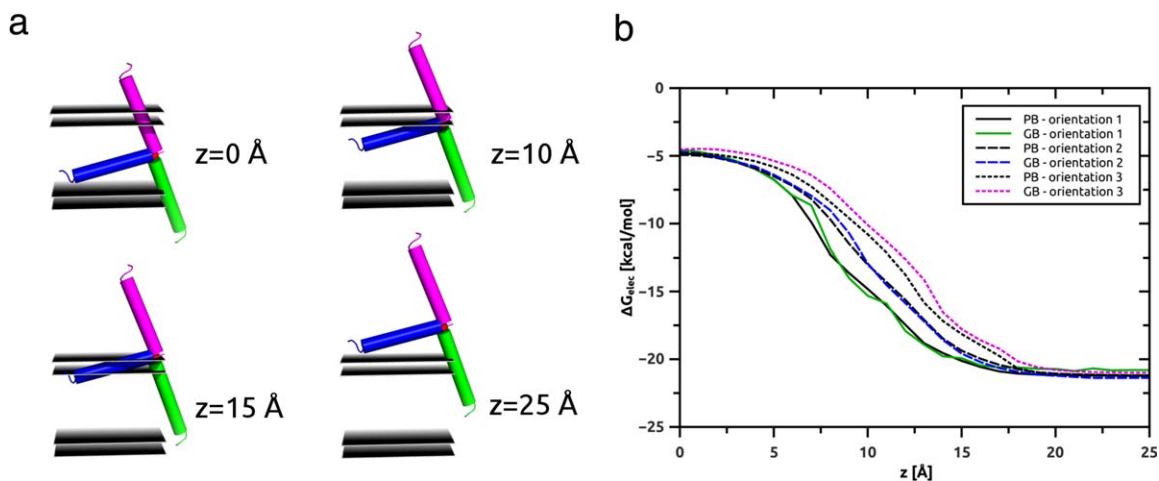


Figure 3. a) Four snapshots of pulling three different oriented native Magainin conformations through the membrane. The z values denote the z position of the single charged atom used in this test, which is located in between the helices at the same position for all three orientations (red sphere). b) Resulting GB based SLIM and PB electrostatic free energy of solvation profiles. Colors of the GB graphs correspond to the colors of the helices in (a).

second ion out of the membrane along the membrane normal. The Spassov like model systematically underestimates the interaction term inside the membrane, while our GB membrane model using the same parameters as in the PB calculations overestimates the interaction by up to 2.19 kcal/mol. Using improved thicknesses and dielectric constants reduces the maximal error to 1.03 kcal/mol.

The overall good agreement to PB calculations presented here validates our approach of decomposing the electrostatic solvation free energy into multiple GB terms proposed in eq. (3). Modifying the dielectric constants and thicknesses of the planar slabs in the GB terms accounts for neglected interactions between induced surface charges at the different interfaces.

Melittin

Melittin of bee venom is an antimicrobial peptide, which causes lysis of bacterial membranes.^[62] It is one of the most widely investigated α -helical membrane peptides^[63–68] and frequently serves as a model system for membrane protein simulations.^[28,29,63,69,70] It is composed of 26 amino acids with charged residues occurring mainly close to the C-terminus of the peptide, while residues near the N-terminus are primarily hydrophobic, whereby Melittin is an amphipathic peptide (for the sequence see Appendix). Due to the residue Pro₁₄ the α -helix is kinked.^[71,72]

Here, we apply the SLIM model to the prediction of the position and orientation of Melittin inside membranes. The orientation depends on certain conditions, such as the protonation of the N-terminus,^[70] peptide concentration,^[62,64] or membrane composition and thickness.^[73] Melittin with a neutral N-terminus is predominantly bound to the membrane interface with a parallel orientation to the membrane plane.^[73,74] Charged residues can act as anchors for the peptide in a perpendicular transmembrane orientation.^[64,72,75,76] This transmembrane orientation plays a crucial role in the

membrane-lytic process.^[62,73] Due to their specific geometry with both, a hydrophilic and a hydrophobic surface, Melittin peptides can cover the membrane surface or stabilize pores with their hydrophilic surface facing the pore interior, making bacterial membranes permeable for water-soluble substances.^[62] X-ray experiments done by Hristova et al. show that the distance of the peptide's center of mass from the membrane center at $z = 0$ Å in dioleoylphosphatidylcholine (DOPC) membranes follows a Gaussian distribution with the peak at $z = 17.5$ Å and a width of 4.3 Å.^[73]

The SLIM model should be able to reproduce the established Melittin properties like the orientation and the center of mass position. Therefore, we carried out Monte Carlo simulations, in which we used the x-ray crystallographic structure (PDB code: 2MLT).^[64,65,77] The N-terminus was deprotonated,

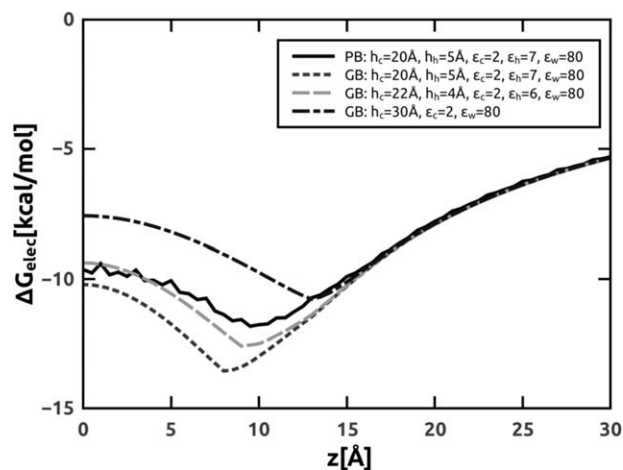


Figure 4. Comparison of the interaction energy between two ions with proton charge placed 4 Å apart along the x direction in the center of the core region. One is pulled out of the membrane along the z direction for PB (solid line), GB with same membrane parameters as PB (dotted line), GB with improved membrane parameters (dashed line), and GB with only one low dielectric slab (dot dashed line).

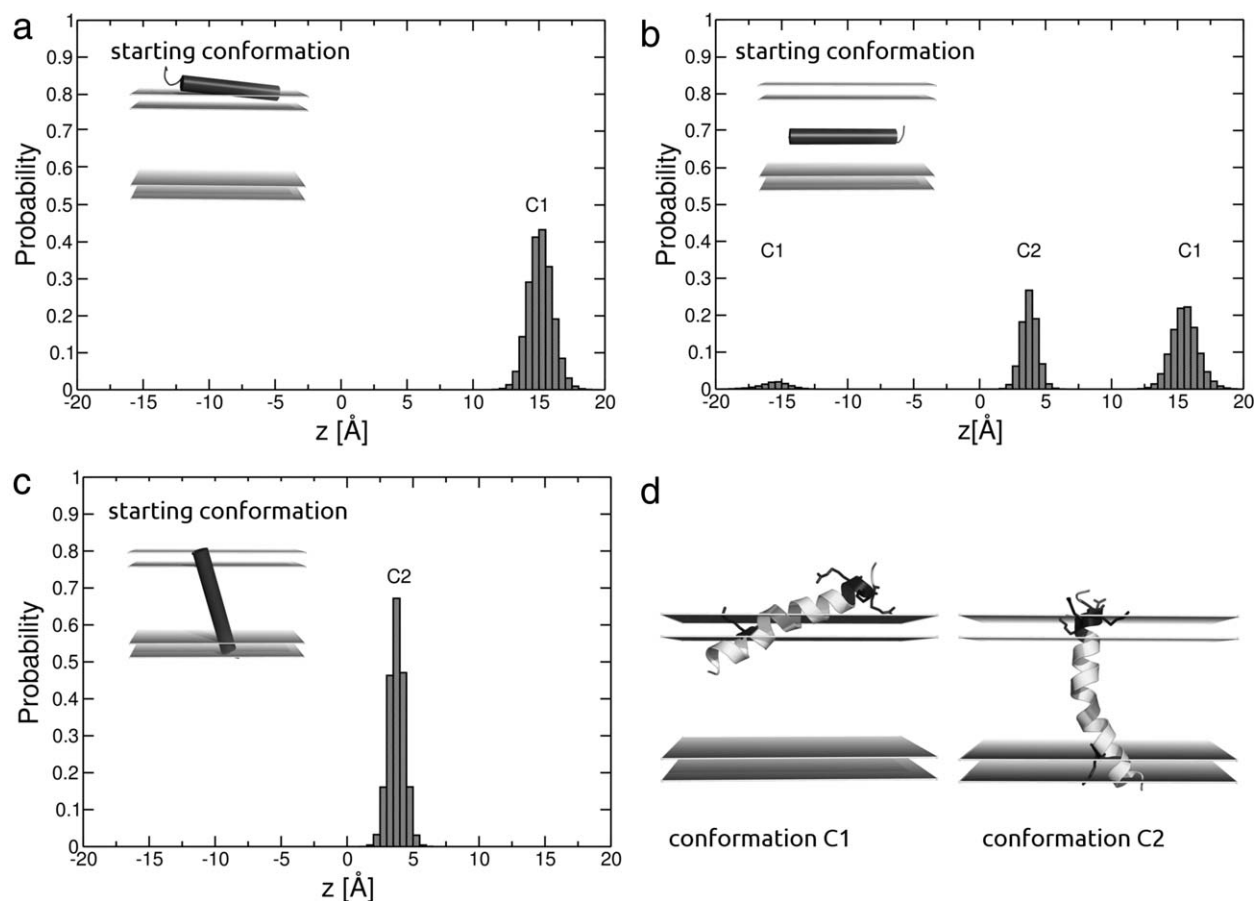


Figure 5. Histograms (a c) of the center of mass probability for Melittin simulations using our proposed membrane model. The corresponding starting conformation is depicted in each histogram. Panel (d) shows exemplary conformations for C1 and C2 peaks in the histograms.

thus, neutral and the C-terminus was charged. The total membrane thickness in our simulations was h_m 30 Å and the surface tension coefficient γ 30 cal/(mol Å²). We performed simulations with three different starting positions and orientations of Melittin and evaluated the resulting location and orientation distributions. The first starting position was chosen similar to an explicit molecular dynamics simulation result of Bernèche et al.^[63] The protein was arranged so that the charged sidechains pointed toward the solvent. For the second and the third starting position, the peptide was moved to the membrane center in a horizontal and a vertical orientation relative to the membrane. For each starting conformation 20 independent simulations were performed.

Figure 5 shows the distribution of the center of mass z -coordinate for the simulations with the three different starting conformations and two exemplary conformations corresponding to the two major peaks in the distributions. For equilibration purposes, the first one million steps of each simulation were discarded in the data analysis.

The center of mass position of Melittin for the simulation that started at the membrane interface is distributed around z 15.1±0.9 Å. During the simulations, all molecules are stabilized there (Fig. 5a). Molecules starting in the membrane center with a horizontal orientation show a different behavior. We find them distributed on both membrane interfaces with

$|z|$ 15.6±1.0 Å, as well as at the membrane center in a vertical membrane spanning orientation with z 3.8±0.6 Å (Fig. 5b). Vertical starting conformations are stabilized in the same conformation, due to the charged residues acting as anchors in the headgroup regions. The distribution is peaked around z 3.8±0.6 Å (Fig. 5c). Figure 5d shows exemplary conformations, which were stabilized during the simulations. They correspond to the orientations, which were found in other studies.^[28,63,70,73] Considering that our total membrane thickness is 30 Å with a 22 Å core region, while according to Nagle et al. the hydrocarbon core of a DOPC membrane is 27.1 Å thick,^[78] our resulting average center of mass of the C1 peaks in Figure 5 is in good agreement with the experimental determined distribution peak at z 17.5±0.2 Å.^[73] The difference in the membrane thickness accounts for the shift of the peak positions.

At the membrane interface, we also find conformations during our simulations, which are excessively kinked near the Pro₁₄ residue (see Supporting Information). Although these conformations could be observed in other implicit membrane simulations, there seems to be no experimental evidence for their existence, wherefore Im et al. argued that its occurrence might be due to the starting conformation.^[28] Our observation of repeated kink formation and stretching of Melittin in our simulations suggests that the cause of this artifact is not the

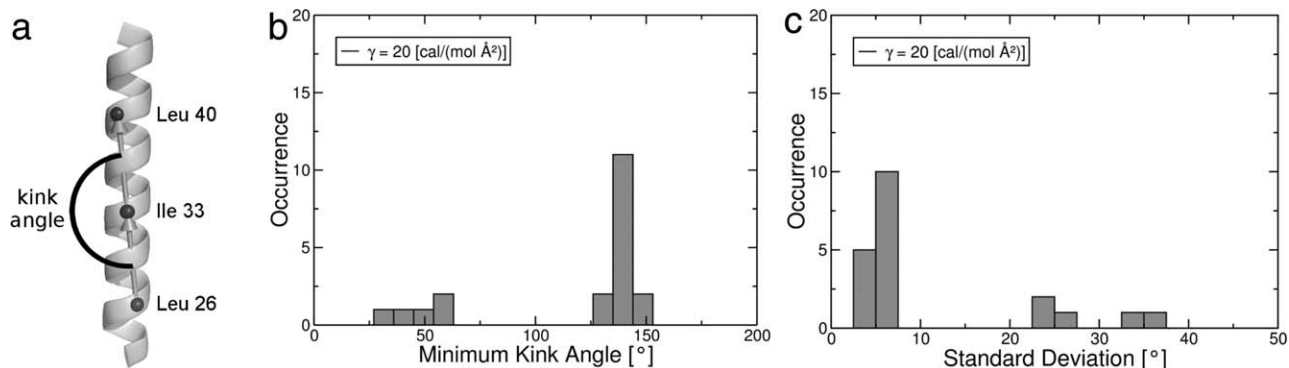


Figure 6. The kink angle for the M2 protein is defined as the angle between the vectors connecting the C_α atoms of residues Leu₂₆ and Ile₃₃ as well as Ile₃₃ and Leu₄₀ (a). The minimum kink angle (b) and standard deviation of the kink angle (c) histograms for the 20 simulations with $h_m = 30 \text{ \AA}$ and $\gamma = 20 \text{ cal/(mol \AA}^2\text{)}$ reveal five simulations with kinked helices apparent by the outliers.

starting conformation. Coarse grained and explicit all-atom molecular dynamics simulations also found excessively kinked “U-shaped” conformations of Melittin.^[79,80] In contrast, recent microsecond molecular dynamics simulations using an explicit membrane representation provide evidence that an excessively kinked conformation is at least not highly populated.^[81] Therefore, it is not clear if this conformation really is an artifact of the molecular force field and membrane model used, or a relevant state in the formation of pores by Melittin, as suggested by Santo and Berkowitz.^[79] In case this “U-shaped” conformation is an artifact, the improved electrostatics of the SLIM model does not prevent its occurrence. Therefore, deficiencies in modeling nonpolar solvation effects are another possible cause. Further investigations will be necessary to provide a clearer picture of this issue and its possible solutions.

A transition of a single Melittin peptide from the membrane bound state to the transmembrane state could not be observed in explicit all-atom molecular dynamics simulations in the microsecond range by Andersson et al.^[81] Irudayam et al.^[82] have investigated the transition of Melittin from a membrane-bound state to a transmembrane state using umbrella sampling. They find that a single Melittin possesses local free energy minima corresponding to either the C1 or the C2 state. This is in agreement with our simulations using the SLIM model. They also find that the global minimum is the transmembrane state for a single Melittin. Since we do not observe any transitions between C1 and C2 in our simulations, it is not clear which of the two states is the global free energy minimum within our implicit SLIM model. Irudayam et al.^[82] also calculated a barrier height between these two states of $13.2 \pm 0.8 \text{ kcal/mol}$, which is associated with the transfer of charged groups through the membrane. Such a high barrier would explain why we, and also Andersson et al., did not observe transitions between the C1 and C2 state, as the corresponding transition states are highly suppressed. Our chosen set of Monte Carlo moves also does not allow a direct jump between the two local minima because of their small extent. Therefore, we are not able to provide free energy differences with our current simulation protocol. This issue can be addressed by using an improved simulation protocol with larger Monte Carlo moves. Since the purpose of the work pre-

sented here is to validate our SLIM model, we will be addressing this issue in another study.

Transmembrane domain of the M2 protein

Another test system for our model is a single transmembrane domain of the M2 protein from the *Influenza A* virus (for the sequence see Appendix), as structurally characterized by Wang et al. (PDB code: 1MP6).^[83] It is a well-studied membrane protein, used both in experimental and theoretical investigations.^[28,84,85] The complete protein forms a tetrameric proton channel,^[86] which is activated by low pH environment through protonation of His₃₇.^[87]

We examine the influence of the membrane thickness h_m and the surface tension γ on the tilt angles of a transmembrane domain of the M2 protein in our model and compare with results of previous studies, where they found different tilt angles for diverse membrane thicknesses, corresponding to the concept of hydrophobic mismatch. This concept describes how proteins or peptides tilt or kink to overcome the energetically unfavorable mismatch between the length of the hydrophobic peptide part and the bilayer thickness.^[88,89] Kovacs et al. studied the influence of lipid bilayer hydrophobic thickness on tilt angles of M2 transmembrane peptide in NMR experiments. They found tilt angles of $37 \pm 3^\circ$ in dimyristoylphosphatidylcholine membranes and $33 \pm 3^\circ$ in DOPC membranes with respect to the bilayer normal.^[90]

We carried out simulations with $h_m = 30 \text{ \AA}$ and different surface tension coefficients $\gamma = 20, 30, 40, 50 \text{ cal/(mol \AA}^2\text{)}$. For each of the four surface tension coefficients, we performed 20 independent simulations where the transmembrane helix was located horizontally inside the membrane at the start of the simulation.

Visual inspection reveals some simulations with kinked helices. In contrast to the Melittin simulations, the kink does not occur at the same residue. Therefore, we define the kink angle for the M2 protein (Fig. 6a) as the angle between the vectors connecting the C_α atoms of residues Leu₂₆ and Ile₃₃ as well as Ile₃₃ and Leu₄₀. This angle should be close to 180.0° for intact helices. In total 8 out of 80 simulations have minimum kink angles lower than 100.0° and much larger fluctuations of the

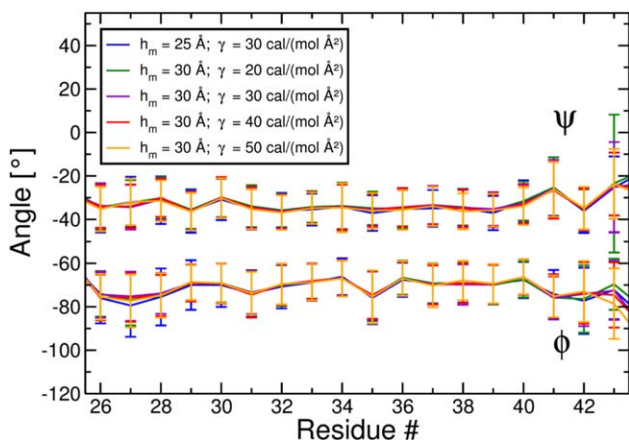


Figure 7. Averaged Φ and Ψ backbone dihedral angles with standard deviations for the transmembrane domain (*Leu*₂₆ to *Leu*₄₃) of the M2 protein as a function of the membrane thickness h_m and the surface tension γ . Data basis for $h_m = 30 \text{ \AA}$ are the 72 simulations with unknicked helices and for $h_m = 25 \text{ \AA}$ the 20 simulations with $\gamma = 30 \text{ cal}/(\text{mol \AA}^2)$, where no knicked helices are present in the simulations.

kink angle compared to the other simulations. For $\gamma = 20 \text{ cal}/(\text{mol \AA}^2)$, five simulations contain knicked conformations, while $\gamma = 30 \text{ cal}/(\text{mol \AA}^2)$ yields one, $\gamma = 40 \text{ cal}/(\text{mol \AA}^2)$ two, and $\gamma = 50 \text{ cal}/(\text{mol \AA}^2)$ zero. Exemplarily, Figure 6 shows histograms for the minimum kink angle (Fig. 6b) and the standard deviation of the kink angle (Fig. 6c) for the 20 simulations with $\gamma = 20 \text{ cal}/(\text{mol \AA}^2)$.

We analyzed Φ and Ψ backbone dihedral angles as a function of the residue number. The resulting average angles and standard deviations for the 72 simulations without knicked conformations are shown in Figure 7. The angles are compatible with an intact alpha helix and agree with values corresponding to the native conformation of the transmembrane domain of the M2 protein.

To enable comparison with experimental data and other implicit membrane models, we use the tilt angle definition of Im

et al.^[28] They define the tilt angle as the angle between the principal axis with the lowest moment of inertia of the backbone heavy atoms of residues *Leu*₂₆ to *Leu*₄₃ and the membrane normal. The principal axis corresponds to the axis of the alpha helix for not too strongly knicked helices. However, this axis is not very descriptive for broken helices, thus, we discard the eight simulations with knicked helices for the following tilt angle analysis. In addition, the first one million steps of all remaining simulations are discarded. With γ increasing from $\gamma = 20 \text{ cal}/(\text{mol \AA}^2)$ up to $\gamma = 50 \text{ cal}/(\text{mol \AA}^2)$, we observe that the average tilt angle increases from 15.8° up to 30.0° as shown in Figure 8a. The large variation of the tilt angles is explained by the shifted balance between nonpolar and electrostatic solvation effects due to the increasing surface tension γ that forces the polar termini regions of the M2 transmembrane domain deeper into the head-group regions as depicted in Figure 8b. The protein accommodates this tension through a higher tilt angle.

Im et al.^[28] also found that the tilt angle increases with the surface tension $\tilde{\gamma}$ in their implicit membrane model. A comparison of the computed tilt angles in Table 1 to the results of Im et al. shows reasonable agreement. However, our tilt angles resulting from the $h_m = 30 \text{ \AA}$ simulations are much smaller than those measured by Kovacs et al.^[90]

Due to the concept of hydrophobic mismatch, we repeated all M2 protein simulations with a thinner membrane of $h_m = 25 \text{ \AA}$, that should cause a higher tilt angle of the transmembrane helix. This time the helix was oriented perpendicular to the membrane interface spanning the membrane at the start of each simulation. In all of these simulations, we do not observe any knicked helices.

The resulting average tilt angles and exemplary conformations are shown in Figures 8a and 8c. Our simulations match our expectations, where we observe larger tilt angles, which increase from 34.0° for $\gamma = 20 \text{ cal}/(\text{mol \AA}^2)$ up to 49.5° for $\gamma = 50 \text{ cal}/(\text{mol \AA}^2)$. An exemplary Φ , Ψ plot proofing helix stability for $h_m = 25 \text{ \AA}$ and $\gamma = 30 \text{ cal}/(\text{mol \AA}^2)$ is shown in Figure 7.

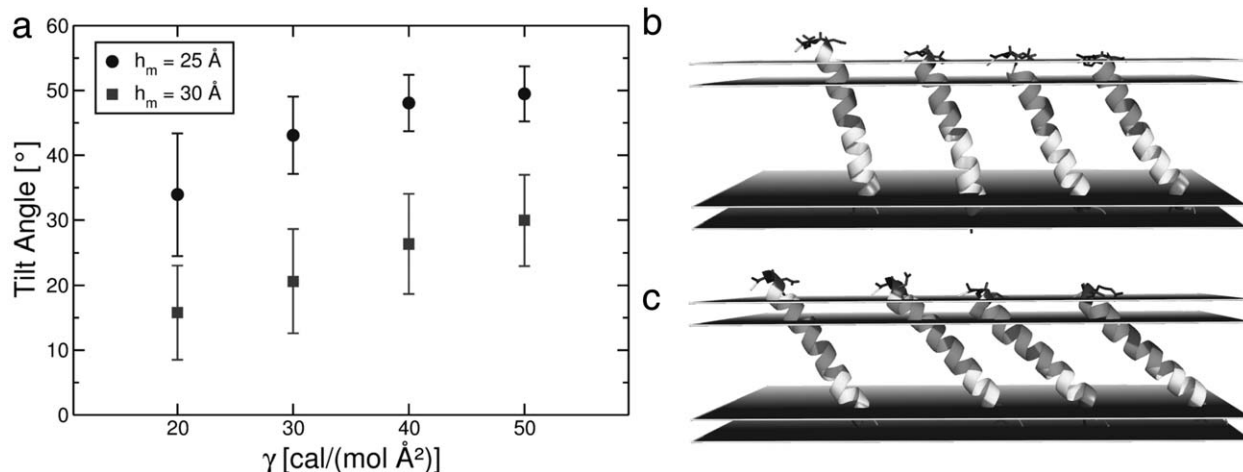


Figure 8. Tilt angle dependence of the transmembrane domain of the M2 protein on the membrane thickness h_m and the surface tension parameter γ in the SLIM model (a). Exemplary conformations [from left to right $\gamma = 20, 30, 40, 50 \text{ cal}/(\text{mol \AA}^2)$] with the average tilt angle in a membrane with $h_m = 30 \text{ \AA}$ thickness (b) and $h_m = 25 \text{ \AA}$ (c).

Table 1. Tilt angle dependence for the transmembrane domain of the M2 protein on the membrane thickness h_m and the surface tension coefficient γ . As a comparison to the SLIM results, the tilt angles of Im et al. are shown.

| | SLIM tilt angles | | | | Im et al. ^[28] tilt angles | |
|---|----------------------|----------------------|----------------------|----------------------|---|----------------------|
| $\bar{\gamma}$ [cal/(mol \AA^2)] | 20.0 | 30.0 | 40.0 | 50.0 | $\bar{\gamma}$ [cal/(mol \AA^2)] | 40.0 |
| h_m 30 \AA | $15.8 \pm 7.3^\circ$ | $20.6 \pm 8.0^\circ$ | $26.4 \pm 7.7^\circ$ | $30.0 \pm 7.0^\circ$ | h_m 29 \AA | $28.5 \pm 5.1^\circ$ |
| h_m 25 \AA | $34.0 \pm 9.4^\circ$ | $43.1 \pm 6.0^\circ$ | $48.1 \pm 4.4^\circ$ | $49.5 \pm 4.3^\circ$ | h_m 25 \AA | $43.1 \pm 3.3^\circ$ |

While these larger tilt angles agree much better with the experimental data, they contrast our previous findings from Melittin, where we argued that our membrane model with h_m

30 \AA is rather thin. Another possibility proposed by Im et al. to explain this discrepancy is the formation of tetramers by the M2 transmembrane domain in the NMR experiments.^[28] The interactions of the transmembrane helices may alter the tilt angles. To investigate the transferability of this argument to our SLIM model, we have chosen the dimer forming Glycophorin A as a simpler but also well-studied test system.

Transmembrane domain of glycophorin A

Glycophorin A (GpA) is a transmembrane protein, the primary sialoglycoprotein of human erythrocyte membranes and forms a dimer due to its specific interactions of the transmembrane α -helices.^[84,91] The three-dimensional structure of the dimeric transmembrane domain of GpA was determined by solution NMR of a 40-residue peptide solubilized in aqueous detergent micelles by MacKenzie et al.^[92] and by solid-state NMR in lipid bilayers by Smith et al.^[93,94]

On the basis of GpA simulations, we investigated if the formation of oligomers does influence the tilt angles of transmembrane helices in the SLIM model and if the dependence of the tilt angle on the surface tension coefficient is less sensitive for dimers than for monomers as suggested by Im et al.^[28]

For the simulations, we used the transmembrane segment Pro₇₁-Ile₉₅ (for the sequence see Appendix, PDB code: 1AFO)^[92] and simulated both a monomer and a dimer in a h_m

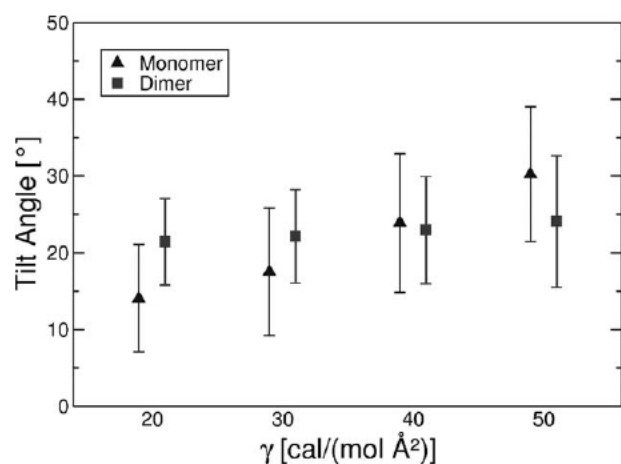


Figure 9. Averaged tilt angles and standard deviations for a monomer and the dimer of the transmembrane domain of Glycophorin A for different surface tension coefficients γ in a h_m 30 \AA thick membrane. For the dimer, the average value includes both chains.

30 \AA thick membrane, each starting in a perpendicular orientation to the membrane interface inside the membrane. The first one million steps of each of the 20 independent simulations for every system and parameter set were discarded when computing the averaged tilt angles and their standard deviations shown in Figure 9.

Similar to the simulations of the M2 protein, we observe increasing tilt angles for bigger surface tension values, which range from $14.08 \pm 6.95^\circ$ (γ 20 cal/(mol \AA^2)) to $30.23 \pm 8.82^\circ$ (γ 50 cal/(mol \AA^2)) for the monomer. The alpha helix remains stable during all simulations. The dimer also remains stable during our simulations, with the average crossing angle varying between 41.2° and 43.1° depending on the surface tension. The standard deviation of the average value is in all cases less than 5° . These results are in good agreement with measurements by MacKenzie et al., who found crossing angles of 40° .^[92]

Comparing the average tilt angles of the monomer with those of the dimer, we observe for $\gamma \leq 30$ cal/(mol \AA^2) larger tilt angles for the dimer. Surface tension values $\gamma \geq 40$ cal/(mol \AA^2) lead to heavier tilted monomers than dimers. In total, the dimer tilt angle varies only by 2.7° compared to 16.1° for the monomer. We conclude that the average tilt angles of the monomer are more sensitive to the surface tension values than the dimer. This observation agrees with the findings of Im et al.^[28]

Furthermore, Petrache et al.^[95] found in their explicit membrane simulations of GpA also much larger tilt angles for dimeric transmembrane helices than for monomeric ones. This suggests that surface tension values $\gamma > 30$ cal/(mol \AA^2) may lead to nonrealistic behavior of GpA in our model. They also observed that the average explicit membrane thickness is up to 2.4 \AA smaller in the dimer simulations than in the monomer simulations.^[95] Due to the fact that our membrane model is not influenced by the inserted proteins, our model parameters should depend on the membrane to be modeled and the protein system to be inserted.

These findings suggest that the discrepancy of the tilt angles between our simulations and experiments for the transmembrane domain of the M2 protein is due to the formation of tetramers in the experiment as proposed by Im et al.,^[28] while we only studied monomers in our simulations.

SLIM simulation performance

We have also compared the simulation performance of our SLIM model in SIMONA to the HDGB model^[29] of Tanizaki and Feig in CHARMM (version 35b^[96]). For the comparison, we used the crystal structure of a bacteriorhodopsin monomer

(PDB code: 1FBB^[97]) with approximately 3500 atoms as the starting conformation and ran short simulations of 1000 molecular dynamics energy minimization or Monte Carlo steps respectively. More details about the performance measurements are available in the Supporting Information.

CHARMM with the HDGB model required 1021 s to complete the simulation, while SIMONA with the SLIM model required only 230 s. Thus, the SIMONA simulation with SLIM achieves about 4.4 times more simulation steps without using any long-range interaction cutoffs.

Conclusion

Results of computational studies using explicit membrane representations suggest implicit membrane models require multiple dielectric regions.^[47] We have presented a new approach to decompose the membrane environment consisting of multiple dielectric regions into a sum of multiple environments consisting of only two different dielectric regions each. These simpler environments can then be treated by GB methods. This approach is used to establish the GB-based SLIM (SIMONA layered implicit membrane) model. As the reproduction of the qualitative features of PB electrostatics is a prerequisite for a correct implicit membrane model, several test cases are used to demonstrate that the SLIM model captures these features, which are not present in previous implicit membrane models.

Further validation of our model by Monte Carlo studies of three well-studied membrane proteins, Melittin from bee venom, a single transmembrane domain of the M2 protein, and the transmembrane domain of the Glycophorin A monomer and dimer, showed that the SLIM model is able to reproduce known properties of these proteins, if the membrane model parameters are chosen properly. These properties include the center of mass position of Melittin, tilt angles of a monomeric M2 transmembrane domain and crossing angles of a Glycophorin A transmembrane dimer. In some cases, heavily kinked conformations of Melittin and the transmembrane domain of the M2 protein were observed, were the former was also found using previous implicit and explicit membrane models.^[28,79,80] Further investigations are necessary to determine the causes of this experimentally unobserved behavior. We have also used these systems to investigate the influence of the membrane model parameters, so that these results may be used as a guide by users in preparing their own simulations. This model will be part of a forthcoming release of the SIMONA software package^[48] available free of charge for academic purposes at <http://www.int.kit.edu/nanosim/>.

Acknowledgments

The authors would like to thank Ivan Kondov and Timo Strunk for careful reading of the manuscript. We gratefully thank the bwGRiD*

*bwGRiD (<http://www.bw.grid.de>), member of the German D Grid initiative, funded by the Ministry for Education and Research (Bundesministerium fuer Bildung und Forschung) and the Ministry for Science, Research and Arts Baden Wuerttemberg (Ministerium fuer Wissenschaft, Forschung und Kunst Baden Wuerttemberg).

project for the computational resources. This work was performed in part on the computational resource bwUniCluster funded by the Ministry of Science, Research and Arts and the Universities of the State of Baden-Wuerttemberg, Germany, within the framework program bwHPC. Author Contributions: JS, CS, MB, and WW designed the research. MB implemented the implicit membrane model. JS and CS parameterized the model, performed PB comparisons, and carried out and analyzed the Monte Carlo simulations. JS, CS, MB and WW drafted and wrote the paper.

Appendix: Amino Acid Sequences

Sequence of Melittin (PDB code: 2MLT)^[64,65,77]:

Gly₁-Ile₂-Gly₃-Ala₄-Val₅-Leu₆-Lys₇-Val₈-Leu₉-Thr₁₀-Thr₁₁-Gly₁₂-Leu₁₃-Pro₁₄-Ala₁₅-Leu₁₆-Ile₁₇-Ser₁₈-Trp₁₉-Ile₂₀-Lys₂₁-Arg₂₂-Lys₂₃-Arg₂₄-Gln₂₅-Gln₂₆

Sequence of the transmembrane region of the M2 protein (PDB code: 1MP6)^[83]:

Ser₂₂-Ser₂₃-Asp₂₄-Pro₂₅-Leu₂₆-Val₂₇-Val₂₈-Ala₂₉-Ala₃₀-Ser₃₁-Ile₃₂-Ile₃₃-Gly₃₄-Ile₃₅-Leu₃₆-His₃₇-Leu₃₈-Ile₃₉-Leu₄₀-Trp₄₁-Ile₄₂-Leu₄₃-Asp₄₄-Arg₄₅-Leu₄₆

Sequence of the transmembrane domain of Glycophorin A (PDB code: 1AFO)^[92]:

Pro₇₁-Glu₇₂-Ile₇₃-Thr₇₄-Leu₇₅-Ile₇₆-Ile₇₇-Phe₇₈-Gly₇₉-Val₈₀-Met₈₁-Ala₈₂-Gly₈₃-Val₈₄-Ile₈₅-Gly₈₆-Thr₈₇-Ile₈₈-Leu₈₉-Leu₉₀-Ile₉₁-Ser₉₂-Tyr₉₃-Leu₉₄-Ile₉₅

Keywords: generalized Born · implicit membrane · proteins · Monte Carlo

- [1] H. Michel, *Trends Biochem. Sci.*, **1983**, *8*, 56–59, DOI:10.1016/0968-0004(83)90390-0.
- [2] M. Hong, Y. Zhang, F. Hu, *Annu. Rev. Phys. Chem.*, **2012**, *63*, 1–24, DOI: 10.1146/annurev-physchem-032511-143731.
- [3] E. Wallin, G. V. Heijne, *Protein Sci.*, **1998**, *7*, 1029–1038, DOI:10.1002/pro.5560070420.
- [4] C. Ostermeier, H. Michel, *Curr. Opin. Struct. Biol.*, **1997**, *7*, 697–701, DOI:10.1016/S0959-440X(97)80080-2.
- [5] B. Byrne, S. Iwata, *Curr. Opin. Struct. Biol.*, **2002**, *12*, 239–243, DOI: 10.1016/S0959-440X(02)00316-0.
- [6] C. R. Sanders, F. Sönnichsen, *Magn. Reson. Chem. MRC*, **2006**, *44* Spec No, S24–40, DOI:10.1002/mrc.1816.
- [7] A. Grossfield, Chapter 5 Implicit Modeling of Membranes, Current Topics in Membranes, Volume 60. Academic Press, 131–157, **2008**.
- [8] R. O. Dror, M. O. Jensen, D. E. Shaw, in Proceedings of the 31st Annual International Conference of the IEEE Engineering in Medicine and Biology Society, EMBC 2009, Minneapolis, Minnesota, USA, Sept 2–6, **2009**; DOI:10.1109/IEMBS.2009.5335057
- [9] P. J. Stansfeld, M. S. P. Sansom, *Structure*, **2011**, *19*, 1562–1572, DOI: 10.1016/j.str.2011.10.002.
- [10] Y. Shan, A. Arkhipov, E. T. Kim, A. C. Pan, D. E. Shaw, *Proc. Natl. Acad. Sci.*, **2013**, DOI:10.1073/pnas.1220843110.
- [11] A. Arkhipov, Y. Shan, R. Das, N. F. Endres, M. P. Eastwood, D. E. Wemmer, J. Kuriyan, D. E. Shaw, *Cell*, **2013**, *152*, 557–569, DOI:10.1016/j.cell.2012.12.030.

- [12] M. Ø. Jensen, V. Jogini, D. W. Borhani, A. E. Leffler, R. O. Dror, D. E. Shaw, *Science*, **2012**, 336, 229–233, DOI:10.1126/science.1216533.
- [13] F. Khalili Araghi, J. Gumbart, P. C. Wen, M. Sotomayor, E. Tajkhorshid, K. Schulten, *Curr. Opin. Struct. Biol.*, **2009**, 19, 128–137, DOI:10.1016/j.sbi.2009.02.011.
- [14] M. Feig, *Methods Mol. Biol. Clifton NJ*, **2008**, 443, 181–196, DOI: 10.1007/978-1-59745-177-2_10.
- [15] S. J. Marrink, A. H. de Vries, A. E. Mark, *J. Phys. Chem. B*, **2004**, 108, 750–760, DOI:10.1021/jp036508g.
- [16] D. H. de Jong, G. Singh, W. F. D. Bennett, C. Arnarez, T. A. Wassenaar, L. V. Schäfer, X. Periole, D. P. Tieleman, S. J. Marrink, *J. Chem. Theory Comput.*, **2013**, 9, 687–697, DOI:10.1021/ct300646g.
- [17] J. C. Shelley, M. Y. Shelley, R. C. Reeder, S. Bandyopadhyay, M. L. Klein, *J. Phys. Chem. B*, **2001**, 105, 4464–4470, DOI:10.1021/jp010238p.
- [18] L. Whitehead, C. M. Edge, J. W. Essex, *J. Comput. Chem.*, **2001**, 22, 1622–1633, DOI:10.1002/jcc.1118.
- [19] M. J. Stevens, *J. Chem. Phys.*, **2004**, 121, 11942–11948, DOI:10.1063/1.1814058.
- [20] P. J. Bond, M. S. P. Sansom, *J. Am. Chem. Soc.*, **2006**, 128, 2697–2704, DOI:10.1021/ja0569104.
- [21] M. G. Saunders, G. A. Voth, *Annu. Rev. Biophys.*, **2013**, 42, 73–93, DOI: 10.1146/annurev-biophys-083012-130348.
- [22] P. Ducarme, M. Rahman, R. Brasseur, *Proteins*, **1998**, 30, 357–371.
- [23] R. G. Efremov, D. E. Nolde, G. Vergoten, A. S. Arseniev, *Biophys. J.*, **1999**, 76, 2448–2459, DOI:10.1016/S0006-3495(99)77400-X.
- [24] R. G. Efremov, D. E. Nolde, G. Vergoten, A. S. Arseniev, *Biophys. J.*, **1999**, 76, 2460–2471.
- [25] N. Ben Tal, A. Ben Shaul, A. Nicholls, B. Honig, *Biophys. J.*, **1996**, 70, 1803–1812, DOI:10.1016/S0006-3495(96)79744-8.
- [26] V. Z. Spassov, L. Yan, S. Szalma, *J. Phys. Chem. B*, **2002**, 106, 8726–8738, DOI:10.1021/jp020674r.
- [27] T. Lazaridis, *Proteins Struct. Funct. Bioinforma.*, **2003**, 52, 176–192, DOI: 10.1002/prot.10410.
- [28] W. Im, M. Feig, C. L. Brooks III, *Biophys. J.*, **2003**, 85, 2900–2918, DOI: 10.1016/S0006-3495(03)74712-2.
- [29] S. Tanizaki, M. Feig, *J. Chem. Phys.*, **2005**, 122, 124706, DOI:10.1063/1.1865992.
- [30] D. Murray, N. BenTal, B. Honig, S. McLaughlin, *Structure*, **1997**, 5, 985–989, DOI:10.1016/S0969-2126(97)00251-7.
- [31] K. M. Callenberg, O. P. Choudhary, G. L. de Forest, D. W. Gohara, N. A. Baker, M. Grabe, *PLoS One*, **2010**, 5, DOI:10.1371/journal.pone.0012722.
- [32] S. Jo, M. Vargyas, J. Vasko Szedlar, B. Roux, W. Im, *Nucleic Acids Res.*, **2008**, 36, W270–W275, DOI:10.1093/nar/gkn314.
- [33] M. B. Ulmschneider, J. P. Ulmschneider, M. S. P. Sansom, A. Di Nola, *Bio phys. J.*, **2007**, 92, 2338–2349, DOI:10.1529/biophysj.106.081810.
- [34] M. Born, *Z. Fr Phys.*, **1920**, 1, 45–48, DOI:10.1007/BF01881023.
- [35] D. Bashford, D. A. Case, *Annu. Rev. Phys. Chem.*, **2000**, 51, 129–152, DOI:10.1146/annurev.physchem.51.1.129.
- [36] M. Feig, C. L. Brooks, *Curr. Opin. Struct. Biol.*, **2004**, 14, 217–224, DOI: 10.1016/j.sbi.2004.03.009.
- [37] G. Hawkins, C. Cramer, D. Truhlar, *Chem. Phys. Lett.*, **1995**, 246, 122–129, DOI:10.1016/0009-2614(95)01082-K.
- [38] M. Schaefer, M. Karplus, *J. Phys. Chem.*, **1996**, 100, 1578–1599, DOI: 10.1021/jp9521621.
- [39] D. Qiu, P. S. Shenkin, F. P. Hollinger, W. C. Still, *J. Phys. Chem. A*, **1997**, 101, 3005–3014, DOI:10.1021/jp961992r.
- [40] M. S. Lee, F. R. Salsbury, C. L. Brooks, *J. Chem. Phys.*, **2002**, 116, 10606, DOI:10.1063/1.1480013.
- [41] A. N. Romanov, S. N. Jabin, Y. B. Martynov, A. V. Sulimov, F. V. Grigoriev, V. B. Sulimov, *J. Phys. Chem. A*, **2004**, 108, 9323–9327, DOI: 10.1021/jp046721s.
- [42] H. Tjong, H. X. Zhou, *J. Phys. Chem. B*, **2007**, 111, 3055–3061, DOI: 10.1021/jp066284c.
- [43] E. Gallicchio, R. M. Levy, *J. Comput. Chem.*, **2004**, 25, 479–499, DOI: 10.1002/jcc.10400.
- [44] G. D. Hawkins, C. J. Cramer, D. G. Truhlar, *J Phys Chem*, **1996**, 100, 19824–19839, DOI:10.1021/jp961710n.
- [45] A. Ghosh, C. S. Rapp, R. A. Friesner, *J. Phys. Chem. B*, **1998**, 102, 10983–10990, DOI:10.1021/jp982533o.
- [46] W. C. Still, A. Tempczyk, R. C. Hawley, T. Hendrickson, *J. Am. Chem. Soc.*, **1990**, 112, 6127–6129.
- [47] H. Nymeyer, H. X. Zhou, *Biophys. J.*, **2008**, 94, 1185–1193, DOI:10.1529/biophysj.107.117770.
- [48] T. Strunk, M. Wolf, M. Brieg, K. Klenin, A. Biewer, F. Tristram, M. Ernst, P. J. Kleine, N. Heilmann, I. Kondov, W. Wenzel, *J. Comput. Chem.*, **2012**, n/a–n/a, DOI:10.1002/jcc.23089.
- [49] B. Roux, T. Simonson, *Biophys. Chem.*, **1999**, 78, 1–20, DOI:10.1016/S0301-4622(98)00226-9.
- [50] J. P. Bardhan, *J. Chem. Phys.*, **2008**, 129, 144105, DOI:10.1063/1.2987409.
- [51] T. Grycuk, *J. Chem. Phys.*, **2003**, 119, 4817–4826, DOI:10.1063/1.1595641.
- [52] J. Chen, C. L. Brooks III, *Phys. Chem. Chem. Phys.*, **2008**, 10, 471, DOI: 10.1039/b714141f.
- [53] M. Brieg, W. Wenzel, *J. Chem. Theory Comput.*, **2013**, 9, 1489–1498, DOI:10.1021/ct300870s.
- [54] K. V. Klenin, F. Tristram, T. Strunk, W. Wenzel, *J. Comput. Chem.*, **2011**, 32, 2647–2653, DOI:10.1002/jcc.21844.
- [55] S. J. Marrink, H. J. C. Berendsen, *J. Phys. Chem.*, **1996**, 100, 16729–16738, DOI:10.1021/jp952956f.
- [56] S. Pronk, S. Páll, R. Schulz, P. Larsson, P. Bjelkmar, R. Apostolov, M. R. Shirts, J. C. Smith, P. M. Kasson, D. van der Spoel, B. Hess, E. Lindahl, *Bioinformatics*, **2013**, 29, 845–854, DOI:10.1093/bioinformatics/btt055.
- [57] V. Hornak, R. Abel, A. Okur, B. Strockbine, A. Roitberg, C. Simmerling, *Proteins Struct. Funct. Bioinforma.*, **2006**, 65, 712–725, DOI:10.1002/prot.21123.
- [58] K. Lindorff Larsen, S. Piana, K. Palmo, P. Maragakis, J. L. Klepeis, R. O. Dror, D. E. Shaw, *Proteins*, **2010**, 78, 1950–1958, DOI:10.1002/prot.22711.
- [59] R. B. Best, G. Hummer, *J. Phys. Chem. B*, **2009**, 113, 9004–9015, DOI: 10.1021/jp901540t.
- [60] W. Im, D. Beglov, B. Roux, *Comput. Phys. Commun.*, **1998**, 111, 59–75, DOI:10.1016/S0010-4655(98)00016-2.
- [61] J. Gesell, M. Zaslhoff, S. J. Opella, *J. Biomol. NMR*, **1997**, 9, 127–135.
- [62] C. E. Dempsey, *Biochim. Biophys. Acta BBA Rev. Biomembr.*, **1990**, 1031, 143–161, DOI:10.1016/0304-4157(90)90006-X.
- [63] S. Bernòche, M. Nina, B. Roux, *Biophys. J.*, **1998**, 75, 1603–1618, DOI: 10.1016/S0006-3495(98)77604-0.
- [64] T. C. Terwilliger, D. Eisenberg, *J. Biol. Chem.*, **1982**, 257, 6010–6015.
- [65] T. C. Terwilliger, D. Eisenberg, *J. Biol. Chem.*, **1982**, 257, 6016–6022.
- [66] R. Bazzo, M. J. Tappin, A. Pastore, T. S. Harvey, J. A. Carver, I. D. Campbell, *Eur. J. Biochem.*, **1988**, 173, 139–146, DOI:10.1111/j.1432-1033.1988.tb13977.x.
- [67] F. Inagaki, I. Shimada, K. Kawaguchi, M. Hirano, I. Terasawa, T. Ikura, N. Go, *Biochemistry (Mosc.)*, **1989**, 28, 5985–5991, DOI:10.1021/bi00440a040.
- [68] T. Ikura, N. G?., F. Inagaki, *Proteins Struct. Funct. Bioinforma.*, **1991**, 9, 81–89, DOI:10.1002/prot.340090202.
- [69] M. Bachar, O. M. Becker, *J. Chem. Phys.*, **1999**, 111, 8672–8685, DOI: 10.1063/1.480207.
- [70] M. Bachar, O. M. Becker, *Biophys. J.*, **2000**, 78, 1359–1375, DOI:10.1016/S0006-3495(00)76690-2.
- [71] A. Pastore, T. S. Harvey, C. E. Dempsey, I. D. Campbell, *Eur. Biophys. J.*, **1989**, 16, 363–367, DOI:10.1007/BF00257885.
- [72] H. Vogel, F. Jöhnig, *Biophys. J.*, **1986**, 50, 573–582.
- [73] K. Hristova, C. E. Dempsey, S. H. White, *Biophys. J.*, **2001**, 80, 801–811, DOI:10.1016/S0006-3495(01)76059-6.
- [74] J. P. Bradshaw, C. E. Dempsey, A. Watts, *Mol. Membr. Biol.*, **1994**, 11, 79–86, DOI:10.3109/09687689409162224.
- [75] H. Vogel, *Biochemistry (Mosc.)*, **1987**, 26, 4562–4572, DOI:10.1021/bi00388a060.
- [76] E. Habermann, H. Kowallek, *Hoppe Seylers Z. Fr Physiol. Chem.*, **1970**, 357, 884–890.
- [77] D. Anderson, T. C. Terwilliger, W. Wickner, D. Eisenberg, *J. Biol. Chem.*, **1980**, 255, 2578–2582.
- [78] J. F. Nagle, S. Tristram Nagle, *Biochim. Biophys. Acta BBA Rev. Bio membr.*, **2000**, 1469, 159–195, DOI:10.1016/S0304-4157(00)00016-2.
- [79] K. P. Santo, M. L. Berkowitz, *J. Phys. Chem. B*, **2012**, 116, 3021–3030, DOI:10.1021/jp212018f.
- [80] S. J. Irudayam, M. L. Berkowitz, *Biochim. Biophys. Acta BBA Biomembr.*, **2012**, 1818, 2975–2981, DOI:10.1016/j.bbmem.2012.07.026.

- [81] M. Andersson, J. P. Ulmschneider, M. B. Ulmschneider, S. H. White, *Bio phys. J.*, **2013**, *104*, L12 L14, DOI:10.1016/j.bpj.2013.02.006.
- [82] S. J. Irudayam, T. Pobandt, M. L. Berkowitz, *J. Phys. Chem. B*, **2013**, *117*, 13457 13463, DOI:10.1021/jp406328d.
- [83] J. Wang, S. Kim, F. Kovacs, T. A. Cross, *Protein Sci.*, **2001**, *10*, 2241 2250, DOI:10.1110/ps.17901.
- [84] I. T. Arkin, *Biochim. Biophys. Acta BBA Biomembr.*, **2002**, *1565*, 347 363.
- [85] L. J. Holsinger, D. Nichani, L. H. Pinto, R. A. Lamb, *J. Virol.*, **1994**, *68*, 1551 1563.
- [86] L. J. Holsinger, R. Alams, *Virology*, **1991**, *183*, 32 43, DOI:10.1016/0042 6822(91)90115 R.
- [87] L. H. Pinto, L. J. Holsinger, R. A. Lamb, *Cell*, **1992**, *69*, 517 528, DOI: 10.1016/0092 8674(92)90452 I.
- [88] J. A. Killian, *Biochim. Biophys. Acta BBA Rev. Biomembr.*, **1998**, *1376*, 401 416, DOI:10.1016/S0304 4157(98)00017 3.
- [89] M. R. R. de Planque, D. V. Greathouse, R. E. Koeppe, H. Schäfer, D. Marsh, J. A. Killian, *Biochemistry (Mosc.)*, **1998**, *37*, 9333 9345, DOI: 10.1021/bi980233r.
- [90] F. A. Kovacs, J. K. Denny, Z. Song, J. R. Quine, T. A. Cross, *J. Mol. Biol.*, **2000**, *295*, 117 125, DOI:10.1006/jmbi.1999.3322.
- [91] J. L. Popot, D. M. Engelman, *Annu. Rev. Biochem.*, **2000**, *69*, 881 922.
- [92] K. R. MacKenzie, J. H. Prestegard, D. M. Engelman, *Science*, **1997**, *276*, 131 133, DOI:10.1126/science.276.5309.131.
- [93] S. O. Smith, R. Jonas, M. Braiman, B. J. Bormann, *Biochemistry (Mosc.)*, **1994**, *33*, 6334 6341, DOI:10.1021/bi00186a037.
- [94] S. O. Smith, D. Song, S. Shekar, M. Groesbeek, M. Ziliox, S. Aimoto, *Biochemistry (Mosc.)*, **2001**, *40*, 6553 6558, DOI:10.1021/ bi010357v.
- [95] H. I. Petrache, A. Grossfield, K. R. MacKenzie, D. M. Engelman, T. B. Woolf, *J. Mol. Biol.*, **2000**, *302*, 727 746, DOI:10.1006/ jmbi.2000.4072.
- [96] B. R. Brooks, C. L. Brooks, A. D. Mackerell, L. Nilsson, R. J. Petrella, B. Roux, Y. Won, G. Archontis, C. Bartels, S. Boresch, A. Caffisch, L. Caves, Q. Cui, A. R. Dinner, M. Feig, S. Fischer, J. Gao, M. Hodoscek, W. Im, K. Kuczera, T. Lazaridis, J. Ma, V. Ovchinnikov, E. Paci, R. W. Pastor, C. B. Post, J. Z. Pu, M. Schaefer, B. Tidor, R. M. Venable, H. L. Woodcock, X. Wu, W. Yang, D. M. York, M. Karplus, *J. Comput. Chem.*, **2009**, *30*, 1545 1614, DOI:10.1002/jcc.21287.
- [97] S. Subramaniam, R. Henderson, *Nature*, **2000**, *406*, 653 657, DOI: 10.1038/35020614.